Electronic Supplementary Information:

Cluster defects in gibbsite nanoplates grown at acidic to neutral pH

Sebastian T. Mergelsberg[a], Mateusz Dembowski[a], Mark E. Bowden[a], Trent R. Graham[a], Micah Prange[a], Hsiu-Wen Wang[b], Xin Zhang[a], Odeta Qafoku[c], Kevin M. Rosso[a], Carolyn I. Pearce[a,c]

[a]Physical Sciences Division, [c]Energy and Environment Directorate, Pacific Northwest national Laboratory, Richland, Washington 99352, USA

[b]Oak Ridge National Laboratory, Oak Ridge, Tennessee 37831, USA

[c]Washington State University, Pullman, Washington 99164

July 19, 2021

S1. Fitting of geometric growth model to BET data

This study used an additional precipitation step not previously published as part of the gibbsite synthesis protocol to produce additional material. Instead of a previously published [ref] 3 day synthesis, the yield of gibbsite material was significantly improved by extending the reaction time to 7 days. Materials from both syntheses were then characterized in order to determine that the extended reaction time did not result in a significant difference in crystallinity or defect density. See Figure S1 for a detailed comparison.

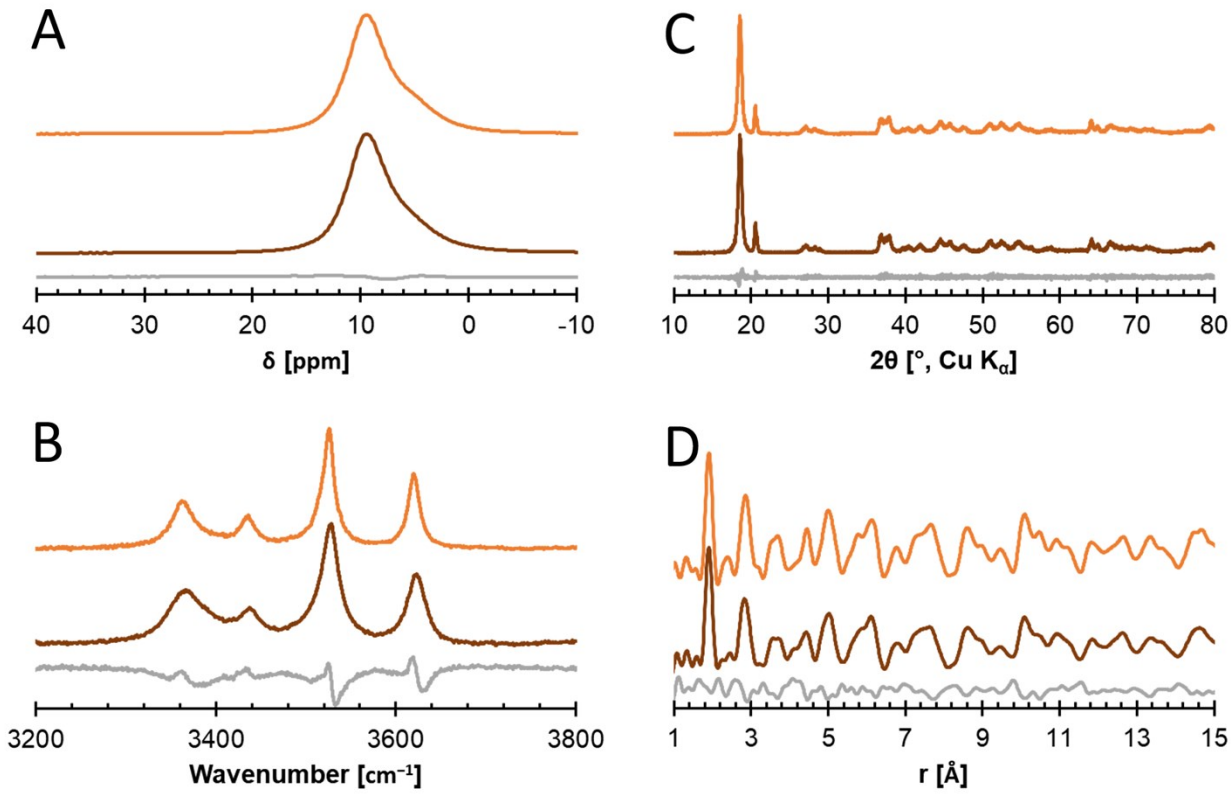

Figure S1. Comparison of 3 day synthesis (orange) previously reported in the literature to the 7 day synthesis (brown) used in this study. Normalized (A) NMR, (B) Raman spectroscopy, (C) XRD, and (D) PDF signals of both synthesis products. The grey line in all graphs represents the differential (7 day – 3 day).

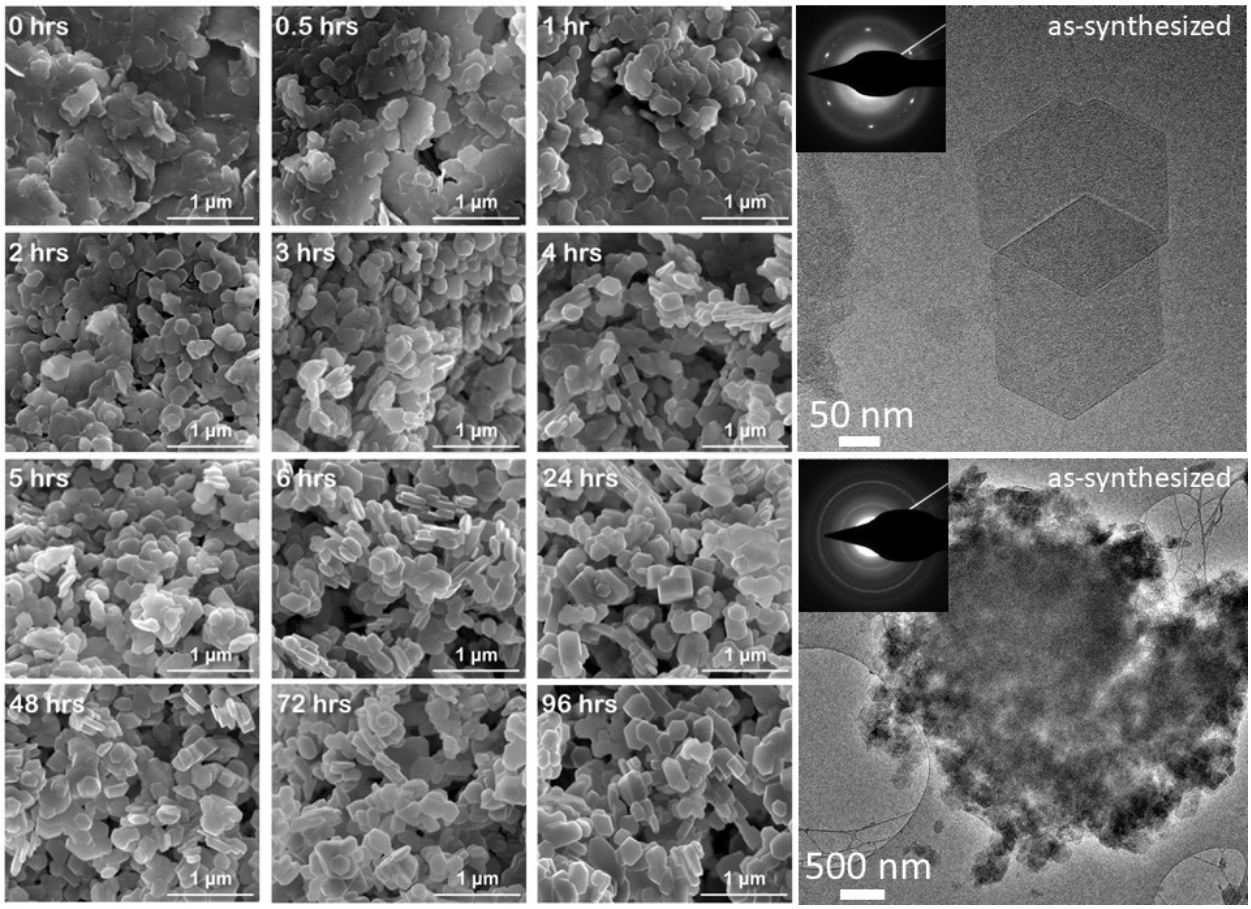

Figure S2. SEM images of gibbsite during different stages of reaction and TEM images of the as-synthesized nanoplates (right). Plate thickness appears to increase continuously, while aggregation of particles seemingly decreases during the reaction.

S2. Fitting of geometric growth model to BET data

To evaluate the average width, height, and growth rate of the gibbsite nanoplates, two geometric growth models were fit to the data. First, we made the assumption that gibbsite nanoplates can be described as free (not overlapping) regular hexagonal prisms with side length a and thickness h. The volume of a hexagonal plate can thus be calculated:

$$A_s = 3\sqrt{3}a^2 + 6ah \tag{S1}$$

Similarly, surface area of a particle is evaluated by:

$$V = \frac{3\sqrt{3}a^2h}{2} \tag{S2}$$

The specific surface area, $\bar{A}_s$ of the nanoplates additionally depends on the material density, ρ, reported as 2.34 g/cm^3 for gibbsite:

$$\bar{A}_s = \frac{A_s}{\rho V} \tag{S3}$$

The first model (Figure S3A) assumes growth only in one direction, along the shortest dimension of initial particles, height h, as suggested by the SEM images (Figure 2AB). The height of hexagonal particles at time t is thus equal to:

$$h = h_o + td_h \tag{S4}$$

where h_o is the initial thickness of gibbsite nanoplates in nm, t is time in hours, and d_h is the linear rate at which h grows, in nm/hour. Substituting equations (S1) and (S2) into (S3) and adjusting for the time dependence of h (S4) gives:

$$\bar{A}_{s1} = \frac{2\left[3\sqrt{3}a^2 + 6a(h_o + td)\right]}{\rho\left[3\sqrt{3}a^2(h_o + td)\right]} = \frac{2}{\rho}\left[\frac{1}{(h_o + td)} + \frac{2}{\sqrt{3}a}\right] \tag{S5}$$

Using a Levenberg-Marquart non-linear fitting algorithm, this model was fit to the BET data to solve for a, h_o, and d. See Table S1 for fitting details.

This first model results in a quickly changing aspect ratio, producing narrow columns, elongated perpendicular to the basal (001) surface, after only a few hours. Because the particles remain platelets ($a >> h$), a second model (Figures 2C and S3, purple line) was needed, which makes the assumption that particles form with a known width and aspect ratio $c = \frac{a}{h}$. Thus, surface area and volume can be computed as follows:

$$A_s = 3\sqrt{3}a^2 + \frac{6a^2}{c} \tag{S6}$$

$$V = \frac{3\sqrt{3}a^3}{2c} \tag{S7}$$

Next, we assumed particles grow by along a from the initial length a_o by rate d_a, along with a change in aspect ratio from c_1 by c_2, as a function of time t:

$$a = a_o + td_a \tag{S8}$$

$$c = c_1 + tc_2 \tag{S9}$$

Substitution of (S8) and (S9) into (S6), (S7), and (S3) yields an equation describing gibbsite particle growth as a function of a changing width and aspect ratio:

$$\bar{A}_{s2} = \frac{\left[3\sqrt{3}(a_o + td_a)^2 + \frac{6(a_o + td_a)^2}{c_1 + tc_2}\right]}{\rho\left[\frac{3\sqrt{3}(a_o + td_a)^3}{2(c_1 + tc_2)}\right]} = \frac{2\left[(c_1 + tc_2) + \frac{2}{\sqrt{3}}\right]}{\rho\left[(a_o + td_a)\right]} \tag{S10}$$

This equation was fit to the data using a Levenberg-Marquart non-linear fitting algorithm to solve for a_o, c_2, and d_a, fixing $c_1 = 6.18 \pm 1.61$, as determined by the first model (Fig. S3). Finally, the initial height h_o, and the growth rate along h, d_h, can be calculated from the fitting results as follows:

$$h_o = \frac{a_o}{c_1} \tag{S11}$$

$$h_o + td_h = \frac{a_o + td_a}{c_1 + tc_2} \tag{S12}$$

Fit results and statistics are summarized in Table S1.

Table S1. Refined parameters from geometric model fits to the BET data (Figures 2 and S2). Errors shown are the 2σ standard errors of the mean. For both models, we report the source of each value and the overall 2σ standard error of the fit, $S_{2\sigma}$.

parameter	Model 1	Model 2
a_o (nm ± $E_{2\sigma}$)	116.40 ± 13.99*	116.39 ± 14.49*
h_o (nm ± $E_{2\sigma}$)	18.83 ± 2.63*	18.83 ± 2.34**
d_h (nm/hour ± $E_{2\sigma}$)	19.92 ± 4.06*	13.52 ± 11.40**
d_a (nm/hour ± $E_{2\sigma}$)	0***	123.09 ± 25.45*
c_1 (± $E_{2\sigma}$)	6.18 ± 1.61**	6.18 ± 1.61***
c_2 ($hour^{-1}$ ± $E_{2\sigma}$)	-3.18 ± 1.63**	1.22 ± 0.37*
$S_{2\sigma}$	1.864	1.864

* refined directly; **calculated from refined values; ***fixed

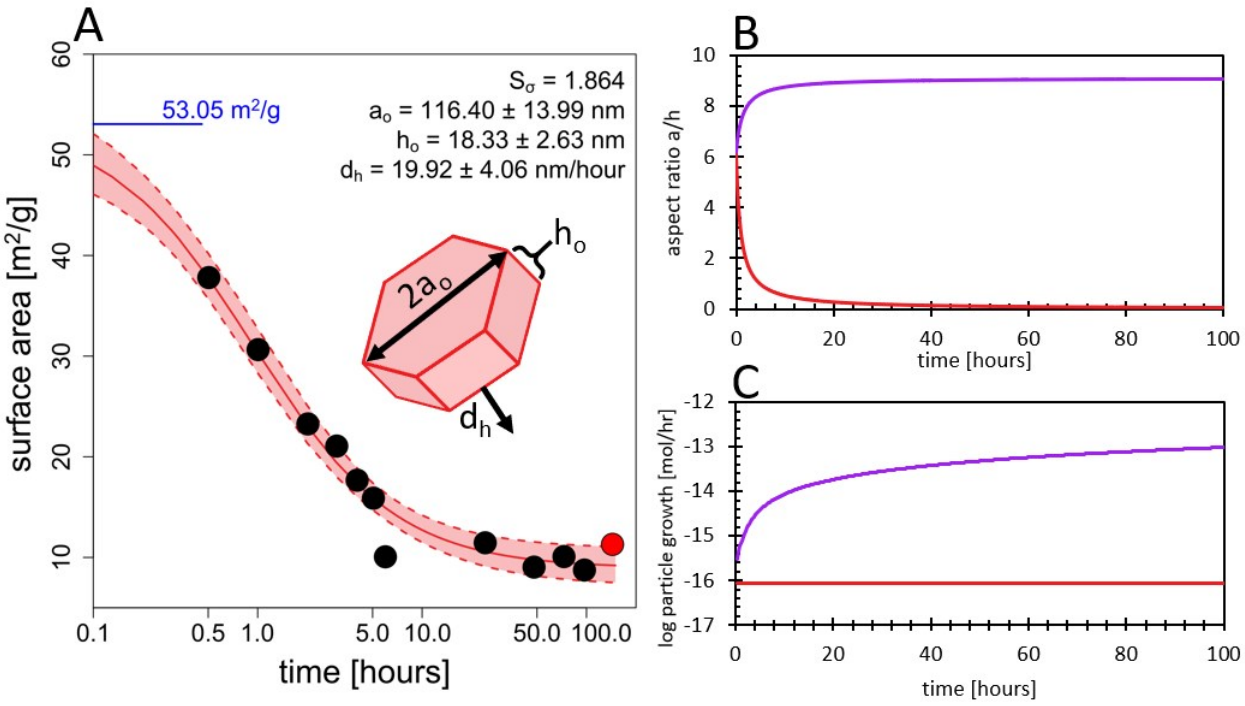

Figure S3. A) Surface area vs. reaction time. The red line represents fit of surface area model 1 to the data using equation S5, assuming hexagonal platelets growing only perpendicular to the basal (001) surface. The standard error of the fit is S = 1.864 and the shaded area represents the 2σ error of the mean (95% confidence interval). B) Aspect ratio a/h as a function of time. C) Particle growth in mol/hr for a single gibbsite nanoplate. Lines for model 1 are shown in red and lines for model 2 in purple.

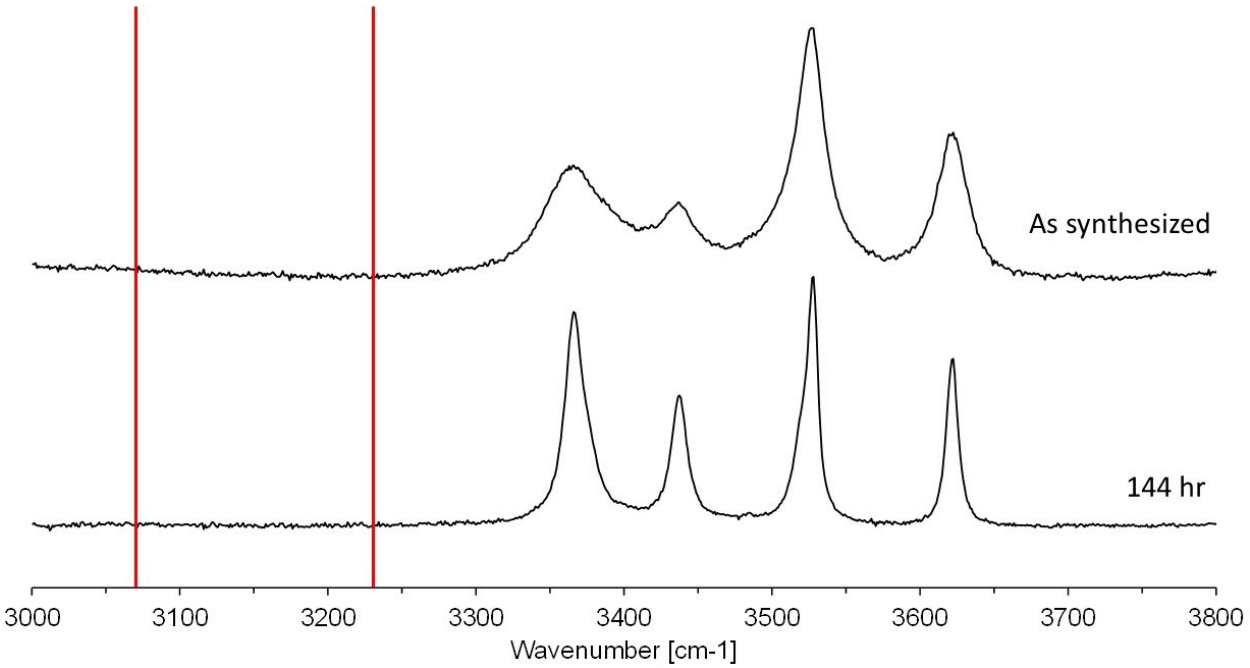

Figure S4. Raman spectra of the hydroxyl stretching region for as synthesized gibbsite and gibbsite after reacting for 144 hr with 3M NaOH at 80°C. Red lines show expected peak positions for boehmite.[1]

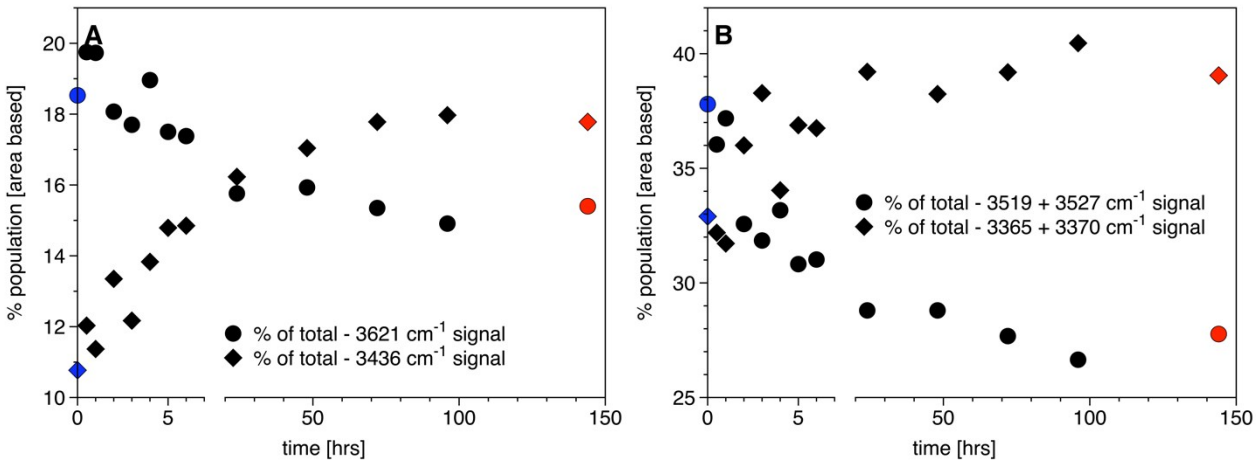

Figure S5. A) Percent population of Raman signal at 3621 cm^{-1} and 3436 cm^{-1} signal as a function of time, which represent the OH stretch within the 001 plane and the OH stretch orthogonal to the 001 plane, respectively. B) Similarly, comparison of percent population of 3519 + 3527 cm^{-1} signals (within 001) vs. 3365 + 3370 cm^{-1} signals (orthogonal to 001) as a function of reaction time. 3519/3527 cm^{-1} and 3365/3370 cm^{-1} signals are represented as a sum due to their considerable overlap.

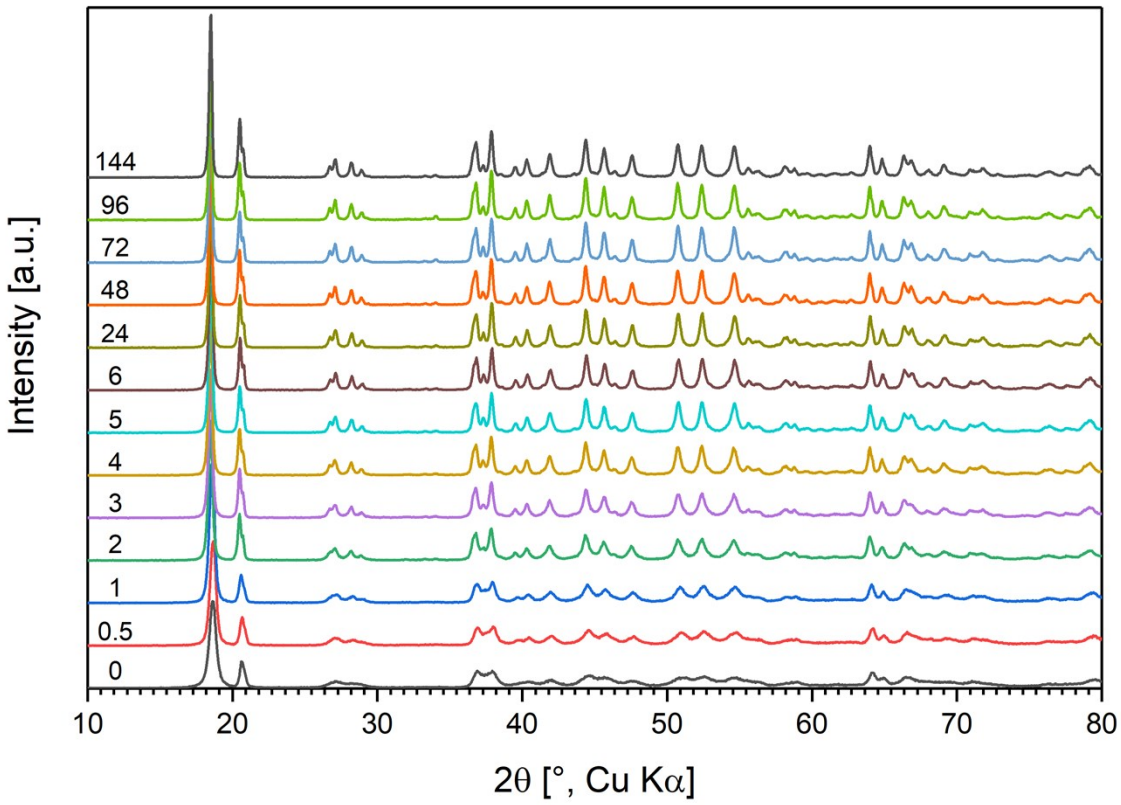

Figure S6. Comparison of XRD results obtained after different aging times (marked at left in hours).

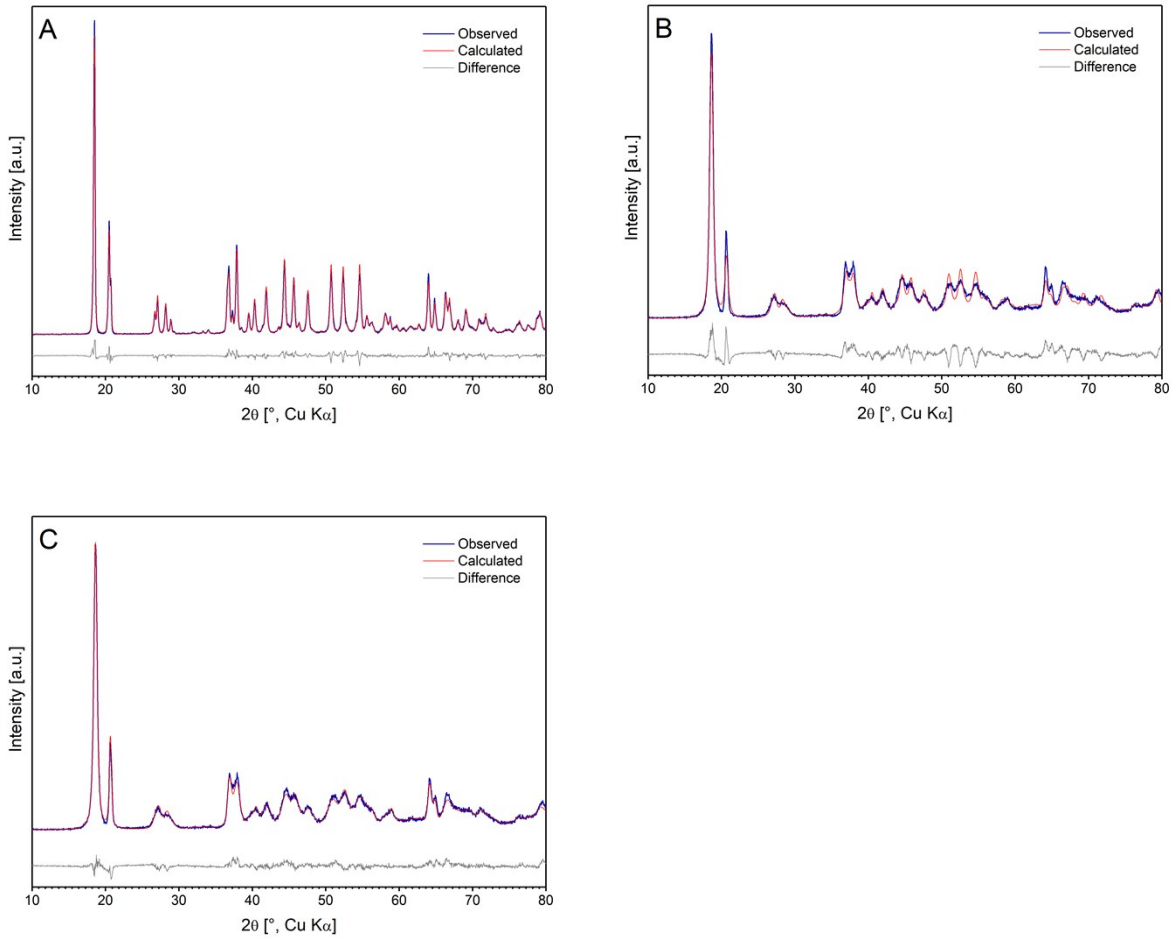

Figure S7. Rietveld refinement fits to the data. A) Aged for 144 hr with line broadening by isotropic crystallite size. B) As-prepared with line broadening by anisotropic crystallite size. C) As-prepared with line broadening by anisotropic crystallite size and anisotropic strain.

S3. XRD Characterization of Starting Material

The bulk nano-gibbsite used in this study was synthesized using a modified version of a previously published method (section 3.1). Powder X-ray diffraction (Figure S1) of the as synthesized material is consistent with nano-gibbsite reported in prior studies and indicates that there are no secondary phases present. A corresponding Rietveld fit that considers peak broadening from isotropic size and strain shows general agreement with the experimental data (Figure S8) but does not account for the observed peak shapes particularly well. Peaks located at approximately 65 degrees 2θ are noticeably sharper than predicted and correspond to the (330) and (600) reflections of gibbsite, both of which arise solely from periodicity within the sheets and include no component of interlayer stacking. This suggests that the intra-layer crystallinity is relatively high when compared to the isotropic broadening model which assumes an equal amount of disorder in all directions. Thus, the initially precipitated gibbsite appears to (1) consist of well-formed sheets and (2) primarily show disorder along the c direction, between sheets. The origin of this disorder is discussed in greater detail in the main text.

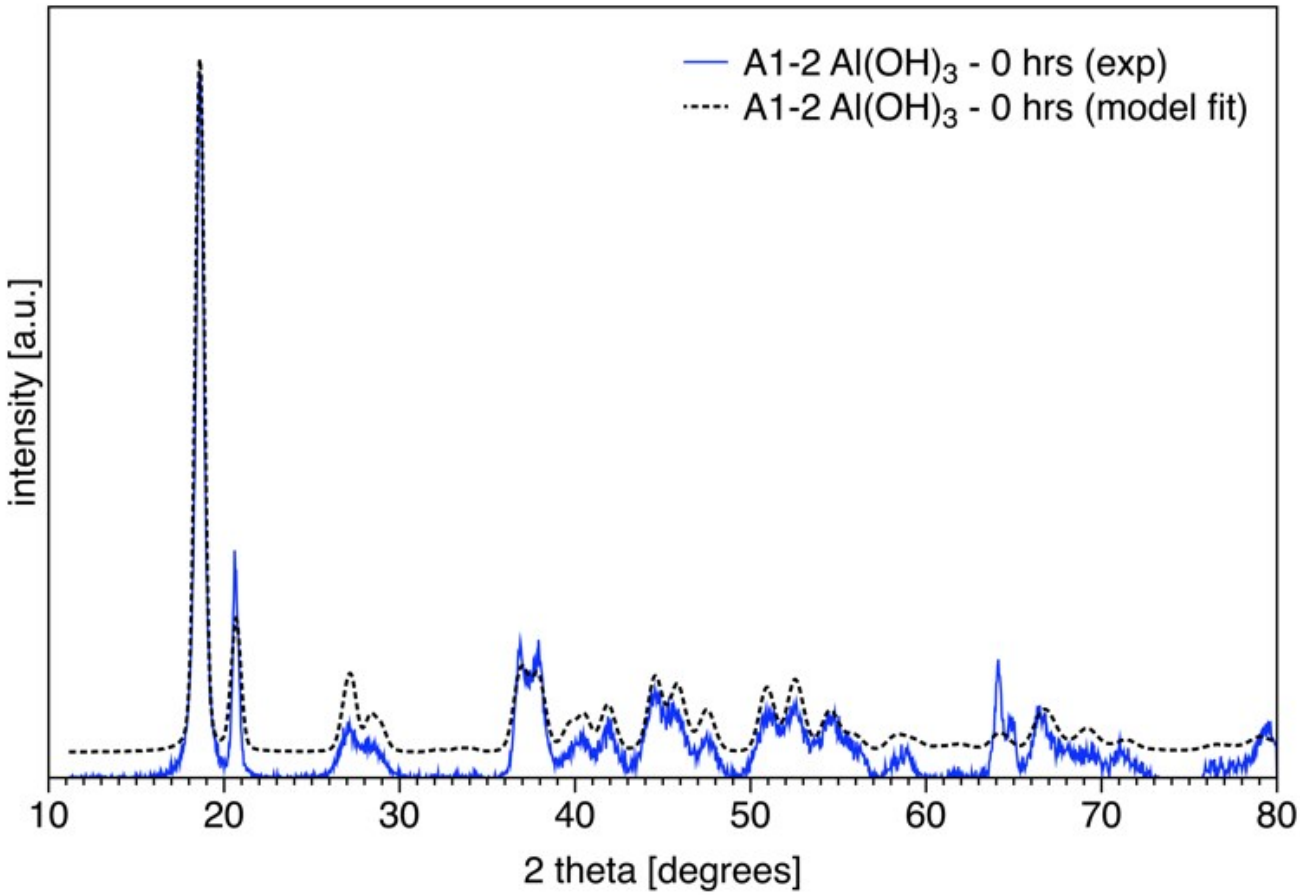

Figure S8. Isotropic size and microstrain model fit to powder XRD data of as-synthesized gibbsite nano-plates.

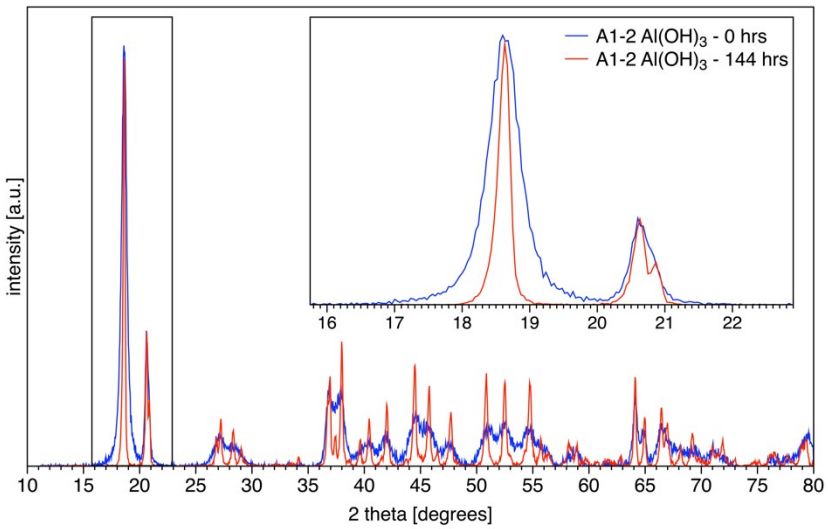

Figure S9. Overlay of as-prepared material (blue trace) with gibbsite aged in 3M NaOH at 80°C for 144 hrs (red trace). The inset highlights the difference in FWHM of XRD peaks between the two samples for the (002) (18.5 degrees), (110) (20.7 degrees), and (200) (20.8 degrees) reflections.

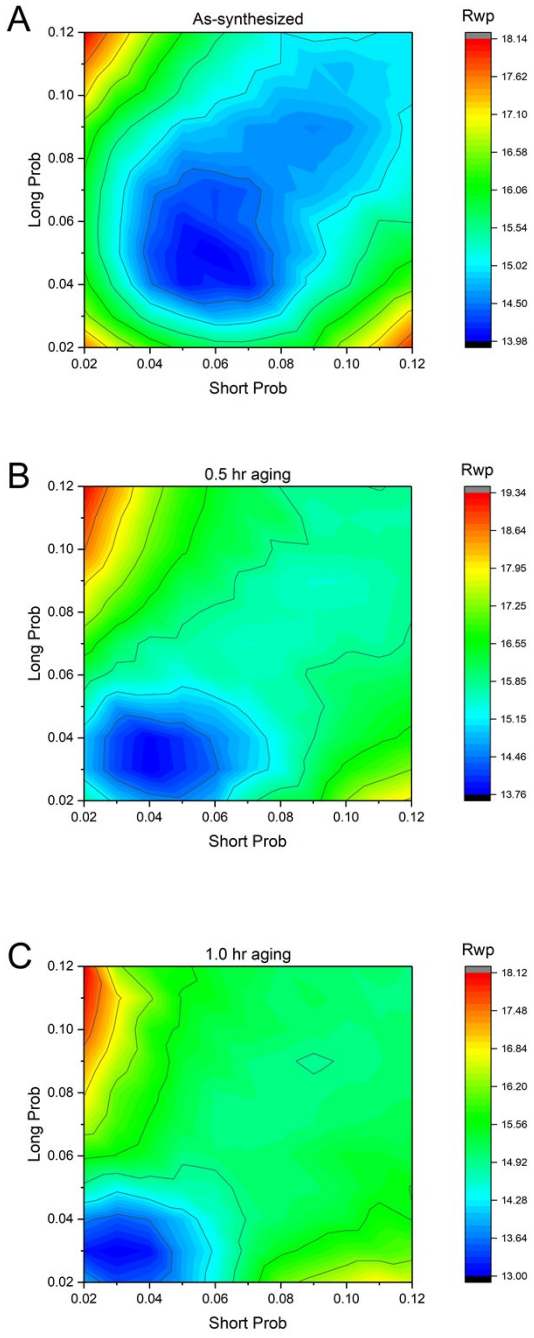

Figure S10. 2D contour plots of mis-stacking probabilities refined by the parameterized model to the XRD data. Better fits are indicated by lower values of R_{wp}. A) At t = 0 hr, the probabilities of the fit are approximately symmetric along the line diagonal, suggesting the probability of closer gibbsite layers is equal to the probability of increased distance between layers. B) After 30 minutes of reaction, the scatter of probabilities has greatly decreased, with a slightly higher chance of closely stacked layers. C) After one hour of reaction, the total probability of mis-

stacking has further decreased, forming a tight distribution close to 3% probability in both the long and short direction.

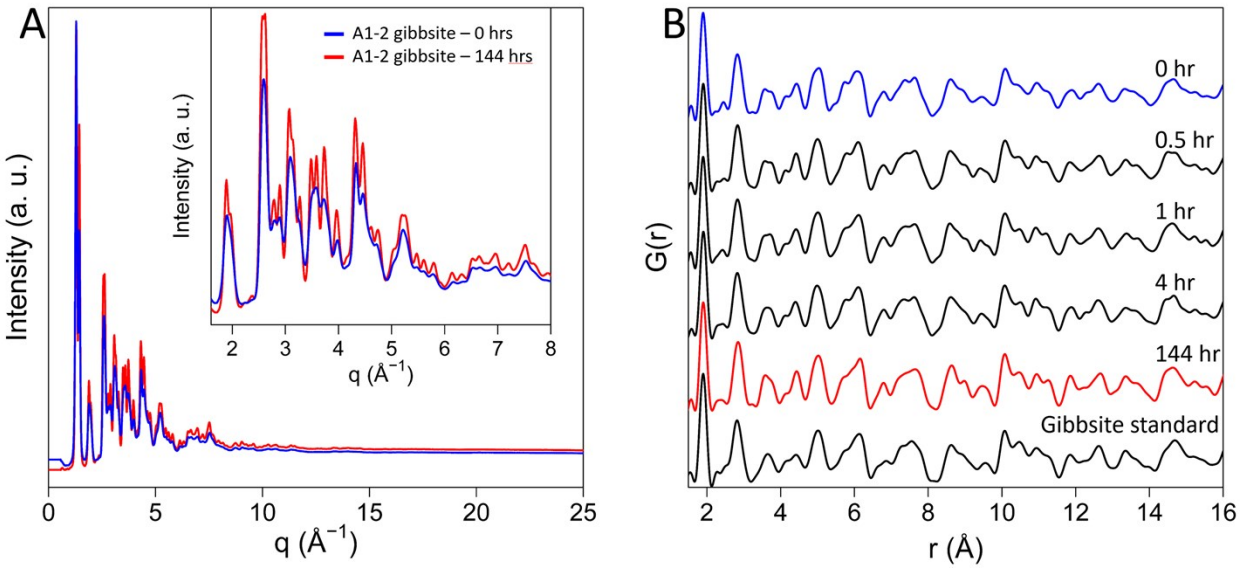

Figure S11. A) Total scattering signal of the initial and final reaction products show a significant increase in crystallinity across q space. The inset highlights the difference in crystallinity for peaks between 1.5 and 8 Å^{-1}. B) PDF analysis reveals the structural disorder on the atomic scale is relatively small in magnitude. The gibbsite standard was calculated from a previously published structure.[2]

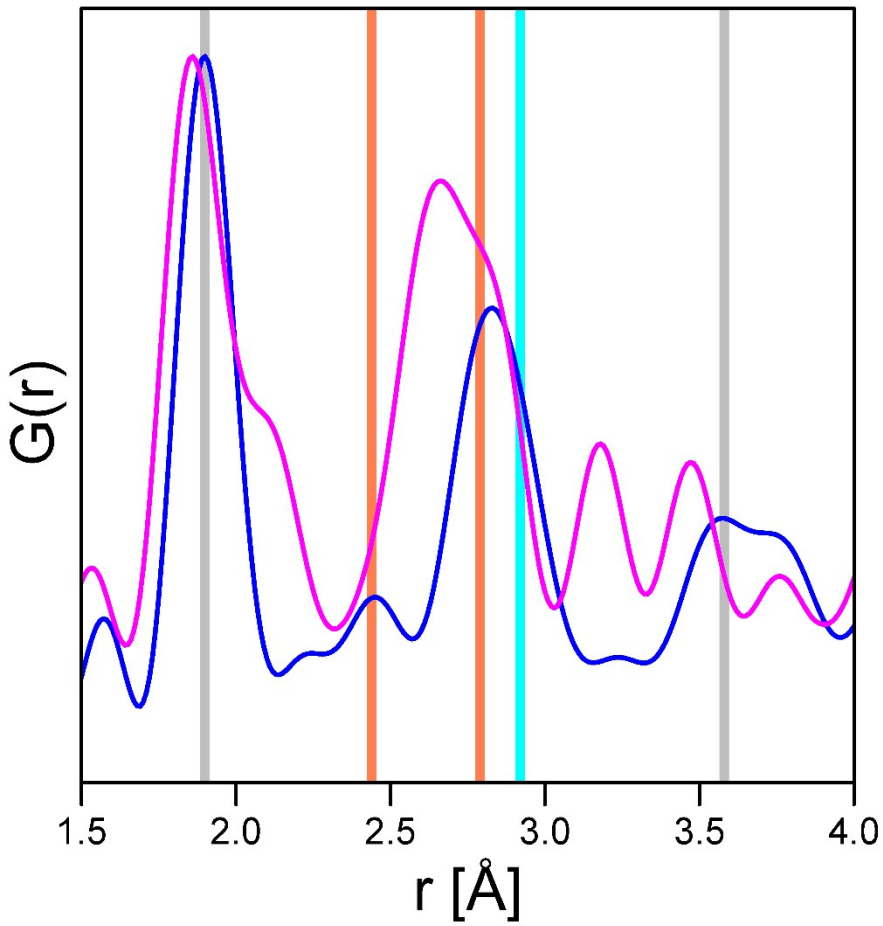

Figure S12. Comparison of the PDF profile of as-synthesized gibbsite nanoplates (blue) to the flat-Al13 cluster only (magenta). Vertical lines represent the position of dominant peaks and represent the Al−O (grey; 1.9 Å, 3.58 Å), O−O (orange; 2.44 Å , 2.79 Å, 3.81 Å), and Al−Al (teal; 2.92 Å) distances.

Table S2. Matrix of structural models generated for the PDF analysis of the gibbsite structure. For each configuration, both types of stacking were modeled, with a range of negative offsets (decreasing the distance between layers). Each configuration additionally was calculated using a chance of 0%, 5%, 10%, 15% or 20% of interstitial sites filled. Note that the center Al site was left vacant in all Keggin-like clusters, as the Al NMR did not indicate the presence of any tetrahedral Al species.

Configuration	⋯ABAB⋯	⋯ABBA⋯	Filled interstitial sites
Two sheets	0 to −0.8 Å	0 to −0.8 Å	0 to 20%
1 unit cell vacant, every 4 unit cells along a, continuous in b	0 to −0.8 Å	0 to −0.8 Å	0 to 20%
2 unit cells vacant, every 4 unit cells along a, continuous in b	0 to −0.8 Å	0 to −0.8 Å	0 to 20%
3 unit cells vacant, every 4 unit cells along a, continuous in b	0 to −0.8 Å	0 to −0.8 Å	0 to 20%
1 unit cell vacant, every 4 unit cells along b, continuous in a	0 to −0.8 Å	0 to −0.8 Å	0 to 20%
2 unit cells vacant, every 4 unit cells along b, continuous in a	0 to −0.8 Å	0 to −0.8 Å	0 to 20%
3 unit cells vacant, every 4 unit cells along b, continuous in a	0 to −0.8 Å	0 to −0.8 Å	0 to 20%
1 unit cell vacant, every 4 unit cells along a and b	0 to −0.8 Å	0 to −0.8 Å	0 to 20%
2 unit cells vacant, every 4 unit cells along a and b	0 to −0.8 Å	0 to −0.8 Å	0 to 20%
3 unit cells vacant, every 4 unit cells along a and b	0 to −0.8 Å	0 to −0.8 Å	0 to 20%
Flat Al_{13} adsorbed to sheet	0 to −0.4 Å	0 to −0.4 Å	N/A
Flat Al_{13} adsorbed to sheet, 3 Al removed facing the sheet	0 to −0.8 Å	0 to −0.8 Å	N/A
Flat Al_{13} adsorbed to sheet, all 6 out-of-plane Al removed	0 to −0.8 Å	0 to −0.8 Å	N/A
Flat Al_6 adsorbed to sheet	0 to −0.4 Å	0 to −0.4 Å	N/A
δ-Al_{13} Keggin adsorbed to sheet	0 to −0.4 Å	0 to −0.4 Å	N/A
ε-Al_{13} Keggin adsorbed to sheet	0 to −0.4 Å	0 to −0.4 Å	N/A

Table S3. Linear combination fits to sub-sections of the PDF signal considered in this study. Unlike the long-range fit presented in Table 1 fits to smaller sections of the PDF profile require an additional component, model ab, which is the structure of gibbsite with a certain difference in stacking density.

Reaction time (hr)	r interval (Å)	144 hr Gibbsite (vol%)	ab_raft_IS_3sol (vol%)	Stacking diff. (Å)	ab (vol%)	Stacking diff. (Å)	Adj. R^2	Red. χ^2
0	1.5 to 4	90.26	--	--	9.74	− 0.2	0.9942	0.00663
	4 to 10	94.05	5.95	− 0.3	--	--	0.9824	0.01800
	10 to 16	90.06	2.97	− 0.3	6.98	− 0.5	0.9458	0.05737
0.5	1.5 to 4	96.5	3.5	− 0.2	--	--	0.9978	0.00229
	4 to 10	89.36	10.64	− 0.3	--	--	0.9862	0.01435
	10 to 16	93.19	6.81	− 0.3	--	--	0.9705	0.03011
1	1.5 to 4	98.46	--	--	1.54	− 0.2	0.9951	0.00623
	4 to 10	93.34	2.53	− 0.3	1.76	− 0.5	0.9902	0.01011
	10 to 16	95.79	4.21	− 0.4	--	--	0.9685	0.03230
4	1.5 to 4	100	--	--	--	--	0.9979	0.00403
	4 to 10	95	4.5	− 0.1	0.5	− 0.5	0.9931	0.00703
	10 to 16	95.29	4.52	− 0.3	0.19	− 0.5	0.9814	0.02246

Table S4. Expected defect density based on the ratio D(r)/G(r) at the location of two major peaks at r = 1.90 Å and r = 2.79 Å, compared to the LCF model results from Table 1.

Reaction time (hr)	1.90 Å (vol %)	2.79 Å (vol %)	Average (vol %)	Model (vol %; Table 1)
0	8.1	7.4	7.7	7.7
0.5	10.0	9.5	9.7	8.7
1	9.9	9.0	9.5	3.8
4	4.6	3.7	4.2	0

REFERENCES

1. H. D. Ruan, R. L. Frost and J. T. Kloprogge, *J. Raman Spectrosc.*, 2001, **32**, 745-750.

2. H. Saalfeld and M. Wedde, *Z Kristallogr*, 1974, **139**, 129-135.